Tensile strength of a compacted vegetated soil: laboratory results and reinforcement interpretation

Alessandro Fraccica[*1], Enrique Romero[1,2] and Thierry Fourcaud[3,4]

[1] Geomechanics Group, CIMNE, Barcelona, Spain

[2] Department of Civil and Environmental Engineering, Universitat Politècnica de Catalunya, Barcelona, Spain

[3] CIRAD, UMR AMAP, F-34398 Montpellier, France.

[4] AMAP, Univ Montpellier, CIRAD, CNRS, INRAE, IRD, Montpellier, France

* Contact details:

Alessandro Fraccica

Geomechanics Group, CIMNE

Department of Civil and Environmental Engineering

Universitat Politècnica de Catalunya - BARCELONATECH

c/ Jordi Girona, 1-3

Campus Nord UPC, Building D-2, Room 308/A

08034 Barcelona - Spain

ORCID: 0000-0003-4304-6765

e-mail: afraccica@cimne.upc.edu

Number of words in the main text: 6488

Number of tables: 5

Number of illustrations: 13

HIGHLIGHTS

- Very few studies have been carried out on the effects of roots on the tensile strength of saturated and partially saturated soils.
- New equipment has been commissioned to test bare and vegetated soils under uniaxial extension.
- Different roots' pull-out mechanisms have been observed depending on whether the soil was saturated or partially saturated.
- Soil tensile strength increase can be interpreted through well-established reinforcement models that consider root's pull-out mechanisms, morpho-mechanical features and soil hydraulic states.
- Tensile strength can be successfully interpreted by an extended shear strength failure criterion for partially saturated soils with roots.

FUNDING

The H2020-ITN project TERRE 'Training Engineers and Researchers to Rethink geotechnical Engineering for a low carbon future' (H2020-MSCA-ITN-2015-675762) provided funding.

ABSTRACT

So far, root reinforcement on soil has been primarily evaluated through direct shear and roots pull-out tests, while the effect of other stress paths and the behaviour at the soil-root interface are still poorly investigated. In this regard, an apparatus with the facility to test soil and roots jointly under uniaxial extension is presented in the paper, together with its first results.

Vegetated samples with *Cynodon dactilon* were tested after one and three months of growth. Soil exhibited a ductile response when close to saturation and a brittle one at drier states within the field capacity domain. The presence of roots increased the material's tensile strength and enhanced its post-peak ductility. Measurements of matric suction and degree of saturation allowed interpreting the results in terms of constitutive stresses within a shear strength failure criterion for partially saturated soils. Even if plant roots critically impacted soil hydraulics, a positive strengthening effect was noticed on its mechanical behaviour.

Roots mechanical and morphological features were characterised after tests. Two well-established root reinforcement models in the literature were used to interpret the results at the phenomenological scale while considering the hydro-mechanical behaviour at the soil-root interface, different root's reinforcement mechanisms and the effect of soil's hydro-mechanical states.

KEYWORDS

Soil tensile strength; root reinforcement; tensile test apparatus; soil-root interface; vegetation effect on soil cracking; partially saturated soils

1. INTRODUCTION

Nowadays, the use of vegetation to mitigate the risk of landslides and erosion phenomena is having a significant interest from researchers and professionals[1-2]. So far, root reinforcement has been evaluated by large direct shear tests, both in situ and in the laboratory[3-7], and by standard or large triaxial equipment[8-12]. New in situ techniques have been proposed to evaluate the stress-strain behaviour in root reinforced-soils, such as pin vane tests and corkscrew method [13-14]. The shear stresses developed in the soil due to the use of these techniques can be directly comparable to those generated in direct shear tests. However, root reinforcement on soil has not been extensively tested along other stress paths – including suction paths – that may lead to soil failure[15-19]. Recently, the effects of climate change on landslides and soil cracking in arid climate conditions have led geotechnical research to focus on the behaviour of soils subject to tensile stress[20-25]. The characterisation of this response may have multiple implications on the current ability to understand and predict the complex interaction between soil and atmosphere. In the case of soil slopes, it leads to a better understanding of the soil response in the upper portions, which may be subjected to horizontal stress reduction and tensile stress paths due to downward mass movements[15]. Moreover, it also allows studying the occurrence of the detrimental effects caused on the soil by tensile cracks linked to shrinkage and swelling cycles[26-29]. So far, there have been some attempts to characterise this behaviour in bare[27,30,31] or fibre-reinforced samples[32-34]. More recently, some investigations have been done quantifying cracks volumes and surfaces in bare and vegetated soils after drying and wetting cycles, finding a good capacity of roots to prevent soil desiccation cracking[35-37]. However, even if these effects suggest an increase of soil tensile

74 strength due to the presence of plants, to the authors' best knowledge, there are few investigations on
75 quantifying the tensile strength of vegetated soils[38]. To this end, an apparatus has been designed and
76 commissioned to characterise the soil's resistance under uniaxial extension and with the possibility of
77 compacting the soil and growing plants inside it.

78 The reinforcement of roots in soils is complex and depends on their morphological and mechanical
79 characteristics and the stresses that develop at the soil-root interface. In this regard, many models have been
80 produced in literature to infer the increase in soil shear/tensile strength due to roots. The first was proposed
81 by Wu et al. (1979)[39]. Within this model, an increase in soil cohesion is correlated with root tensile strength
82 and area ratio ($RAR = A_{roots}/A_{soil}$), while neither soil-root interface friction nor soil hydro-mechanical state was
83 considered. More recent studies confirmed that this model is overpredicting root reinforcement[40-41], as it
84 assumes all the roots to be perpendicular to the zone of shear surface and break at the same time. Coppin
85 and Richards (1990)[42] observed two possible failure mechanisms causing root failure: breakage and slip-out.
86 In the former case, roots' contribution to soil strength increase depends on their tensile resistance, and in
87 the latter, particularly on friction developing at the soil-root interface. Pollen (2007)[43] observed that root
88 breakage was more likely to occur in roots when they were embedded in slightly saturated soil, whereas pull-
89 out mainly was occurring in nearly saturated soil, suggesting the existence of a water content threshold value
90 that distinguishes the probability of occurrence of the two cases. Pollen and Simon (2005)[41] developed a fibre
91 bundle model including the concept of progressive failure in roots but neglecting friction at the soil-root
92 interface. Schwarz et al. (2010)[44] enhanced this model, including roots' geometrical and mechanical features
93 and a soil-root friction's law, even if the effect of soil moisture was not considered. Their model involves
94 knowing roots statistical distributions and performing iterative calculations to determine stresses and
95 displacements (and/or deformations) in roots. Hence, it might be complicated to use when few roots
96 parameters are known.

97 In summary, some models have the theoretical framework for including the soil-root interface behaviour and
98 the effect of soil hydro-mechanical states on root reinforcement, but these effects have not been
99 quantitatively assessed through experiments, in a coupled way and in-depth. Hence, the objectives of this

paper are threefold: a) presenting novel results concerning the effect of vegetation on the tensile strength of silty sand, b) interpreting the vegetated soil's tensile tests at different hydraulic states incorporating a failure criterion for partially saturated soils, and c) exploring and characterising root features, as well as soil hydraulic states, linked to the soil reinforcement mechanisms (breakage and slippage). The results are finally interpreted through well-established literature models for root reinforcement: one considering root tensile strength full exploitation and breakage[39] and the other bearing in mind friction forces at the soil-root interface during root slippage[44]. These two models were combined into one equation, which was calibrated based on this experimental campaign.

2. MATERIALS AND METHODS

2.1. Equipment for tensile tests

The equipment for testing soil under direct tension is made up of two cylindrical moulds of inner diameter 100 mm and height 60 mm (Figure 1). These moulds are held together by two L-shaped pieces, which are needed to contain the soil during its compaction. These removable pieces will allow generating a soil "bridge" linking the soil compacted in the moulds. Given the shape and the narrow size of the bridge (width: 50 mm and length: 32 mm, Figure 1), the tensile crack is expected to be generated right inside it. Therefore, a rounded shape was given to the ends of the two cylindrical moulds to facilitate 3D printing and to smooth possible stress concentrations during the tensile tests (i.e., arching effects, stress concentration due to angular shapes, confining stress increase due to soil-moulds interaction). Particle Image Velocimetry will be presented in the discussion to confirm the effectiveness of this design choice. Finally, grooves have been printed on the inner base of the equipment to enhance adherence with soil.

All the pieces were 3D printed with ABS thermoplastic polymer that has a tensile strength of 28 MPa and an elastic modulus close to 1 GPa[45] still with a very low density (1.05 Mg/m^3) and water absorption in the order of 0.2-0.4% after 24 h of exposition to water[46]. These hydro-mechanical features make the printed polymeric material suitable for this study. One of the moulds is connected to a low-capacity load cell (RSC-1 type, Remberg, Spain, with a range of 500 N and resolution 0.2 N) and the other container to a motor controlling its displacement rate (Starvert-i, Omadisa, Spain). An LVDT (D5-200AG, RDP Electronics, UK, with a range of

10 mm and precision 50 μm) has been connected to this mould to record its horizontal displacement. The moulds are placed on ball-bearing rails with reduced friction (calibrated dynamic friction coefficient 0.002).

2.2. Soil compaction and roots growth

The tested soil has been classified as silty sand by the USCS (Figure 2). Its physical properties are detailed in Table 1. It has been retrieved from the Llobregat Delta in Barcelona (Spain) with a high gravel fraction and sieved at 4.76 mm (Figure 2) to ensure a reasonable ratio between the maximum grain size and the width of the mould's bridge (i.e., 1:10) and allowing its compaction within the equipment. The same ratio recommended for direct shear tests was adopted[47], assuming that tensile failure is ruled by shear strength and developing on a shear surface[30]. Moreover, this ratio is in good agreement with those used by Nahlawi et al. (2004)[48] and Stirling et al. (2015)[29]. The original soil has been used to build an instrumented full-scale embankment to monitor soil-vegetation-atmosphere interactions[49-50].

The sieved soil was statically compacted within the moulds in two layers, each one of final height 20 mm. A spatula created scarifications on the upper surface of the first compacted layer to ensure a good interlocking and continuity with the upper layer. The initial water content w = 15% and dry density ρ_d = 1.6 Mg/m^3 are indicated by point A in in Figure 3 (degree of saturation S_r = 0.61, matric suction s = 40 kPa, void ratio e = 0.67). The total vertical stress imposed on compaction to the material was (100 ± 13) kPa. Due to dry side compaction close to the optimum of the standard Proctor test (Figure 3), the soil structure resulted in a double-porosity type: this ensured enough macro-pores for root growth[12,51]. Subsequently, the samples have been wetted under unconfined conditions to induce plant development (point B in Figure 3, w = 21%, S_r = 0.84, matric suction s = 1 kPa). Soil matric suction was monitored, throughout the process, with a ceramic tip tensiometer (T5x, UMS, Germany) positioned at 70 mm from the central section of the equipment. The wetting-induced volumetric deformations were checked by a Vernier Calliper (Mitutoyo, resolution 0.02 mm) in correspondence to six points well referenced on the samples' surface, and found negligible (i.e., lower than 0.3%). Then, seeds of *Cynodon dactilon* were introduced in 18 soil samples through 2 mm deep and 5 mm in diameter holes, which have been dug with a soil mini-corer, spaced 40 mm apart[51]. The soil's hydraulic state was kept at point B (Figure 3) using an automatic irrigation system during plant growth. The water

content for root growing (i.e. w = 21%) was initially evaluated by oven checking[52] two soil sub-samples from each mould and then by weighing (resolution 0.1 mg) the moulds daily. Moreover, a tensiometer monitored matric suction during root growth (i.e. s = 1 kPa) twice a day. Plants were left to grow between 1 and 3 months, exposed to sunlight. For the sake of comparison, 14 soil samples were left fallow and subject to the same hydraulic path.

2.3. Tensile tests

After roots growth, the samples were left to dry in an atmosphere-controlled room (T = 20°C and RH = 50%) until reaching the desired suction/water content within the field capacity domain (points between B and C in Figure 3). Samples were then wrapped in plastic film for three hours in the darkness to equalise soil suction and stop the plant's transpiration process. After fixing the moulds on the rails, the L-shaped pieces were removed, letting the soil bridge itself connect the two containers (Figure 1). The container linked to the motor was finally pulled at a constant displacement rate (0.080 mm/min) until reaching a displacement of around 5 mm. All the previous procedures and the tensile tests were carried out at the same controlled-atmosphere conditions.

2.4. Stress and state variables assessment

Water content, void ratio and matric suction were evaluated and monitored during each tensile test. Four soil samples were retrieved for water content evaluation by oven-drying[52]: two before and two after each test (a mean water content was considered). A visual inspection was done on the samples to avoid roots being placed in the oven for soil water content measurement.

Matric suction was monitored throughout each tensile test by a ceramic tip tensiometer, installed at a depth of 20 mm and positioned 70 mm far from the central section of the equipment, in the mould linked to the load cell (i.e. not pulled by the motor) to avoid suction oscillations due to sensor's susceptibility to vibrations (Figure 1). Matric suction observed at the peak tensile stress was chosen for further analyses, given that the average difference between initial and final matric suction was, in the tests, in the order of (5 ± 2) kPa.

The void ratio was calculated using paraffin wax tests[53] and water content measurements carried out at the end of each test. One cube of soil was extracted out of the bridge of each tested specimen with a spatula. A visual inspection has ensured the integrity of the extracted cubes. Once the mass and volume of the cubes and the water content were determined, the void ratio was evaluated for fallow soils. However, these variables were insufficient to calculate the void ratio of vegetated soil's cubes. Thus, the vegetated cubes were destroyed after paraffin tests to weigh the roots and measure their volume. The first measurement was carried out with a 0.1 mg resolution balance, and the latter was done by pycnometry (resolution 10 mm^3). Once these additional variables were determined, it was possible to calculate the volume of voids and solid particles separately, and thus the void ratio and the degree of saturation. According to Muir Wood et al. (2016)[54] and Fraccica (2019)[12], the volume of roots V_{roots} was considered herein as an external phase (i.e. neither as a solid phase nor belonging to the volume of the voids). This phase separation allowed observing the effect of roots on soil structure (roots-generated pores) and better assessing the water retention properties of the soil (i.e., differentiating the water that affects the hydro-mechanical response of the soil from that stored in the roots).

2.5. Roots morpho-mechanical characterisation

Three main partitions have been identified within each sample (Figure 4a), and root morpho-mechanical traits were assessed separately for the three. Finally, the traits presented here and considered in the reinforcement model were those observed in the bridge zone, as tensile cracks always occurred in that partition. Fraccica (2019)[12] proposed a correlation between *Cynodon dactilon*'s roots tensile strength and diameter, which was used in this study. The identification of broken roots was made by visual inspection only through the tensile crack. When tests finished (i.e. at a displacement of 5 mm), the roots still crossing the crack were cut by scissors to separate the moulds and measure the root diameters within the crack, using the calliper (Figure 4b). In this way, the $RAR = A_{roots}/A_{soil}$ and $RAR_b = A_{b,roots}/A_{soil}$ ($A_{b,roots}$ area of broken roots) were inferred. The roots that were observed to break after a displacement of 1 mm (minimum displacement to see through the crack) or were cut by scissors at the end of the test were not considered *"broken"* in the computation of the RAR_b. In this manner, only the broken roots that contributed to the soil peak strength

(i.e. between 0 and 1 mm of displacement) were considered within this parameter. Apart from *RAR* and RAR_b, measurements of the root traits were performed after breaking the samples' partitions (Figure 4a) and washing soil to recover the roots at the end of each tensile test (Figure 4c). Root lengths, diameters and branching point distances were measured by a calliper (resolution 0.02 mm, Figure 4d), while root volumes were measured by pycnometry (Figure 4e). Root length was defined as the distance between the plant stem and the tip for vertical roots, and the distance between the tip and the junction with the higher-order root for branches. Broken roots were treated/measured as different roots. A detailed summary of the morphological and mechanical traits considered in this study is presented in Table 2.

3. RESULTS

3.1. Void ratio and retention behaviour

The evolution of the void ratio with increasing matric suction is shown in Figure 5. At the end of each tensile test, paraffin wax tests allowed evaluating roots' contribution in increasing the volume of macro-pores within the soil. The root volume ratio R_v was defined as the volume of roots V_{roots} normalised by the volume of solid particles V_s from which it was retrieved ($R_v = V_{roots}/V_s$, Table 2). This volumetric variable could be easily linked to changes in soil porosity generated by roots growth. Indeed, at the same matric suction, the more R_v observed within the paraffined soil, the higher the void ratio was to the fallow soil condition. This observation is in line with Fraccica et al. (2019)[51] and Carminati et al. (2013)[55], who detected fissures in dry soils around the primary (vertical) roots, but yet a good contact between soil and lateral (sub-horizontal) roots, thanks to the sticky mucilage produced in those parts of the root system. The alteration of this state variable due to roots growth/natural fibres induced a reduction in the retention capacity of the soil, as observed in Figure 6, and as already reported by Fraccica (2019)[12] (relative compaction to Standard Proctor, *RC* = 84%, Clay Fraction, *CF* = 8%, dry density ρ_D = 1.60 Mg/m^3, as this study), Ni et al. (2019)[56] (*RC* = 90%, *CF* = 24%, ρ_D = 1.52 Mg/m^3) and Ng et al. (2014)[57] (*RC* = 70%, *CF* = 12%, ρ_D = 1.31 Mg/m^3). Results correlate well with those observed in situ by Oorthuis et al. (2018; 2021)[49,50], for the same soil and similar compaction levels. The results observed in this study for bare soil were fitted according to the mono-modal water retention curve proposed by Romero and Vaunat (2000)[58] (calibrated parameters: $\alpha_{RV} = 2.5 \cdot 10^{-3}$ MPa^{-1}, n_{RV}

228 *= 0.32, m_{RV} = 14.02, $a_{r,RV}$ = 200 MPa).* Fitting vegetated soil retention measurements requires more advanced
229 bi-modal constitutive laws, in which the retention capacity also depends on root morphological traits (out of
230 the scopes of this study). For this reason, the bi-modal[59] water retention curve proposed by Fraccica (2019)[12]
231 was used for vegetated soil measurements (Figure 6). This model represents the change in water retention
232 behaviour due to the presence of a given amount of roots volume (R_v *= 0.007*), considering void ratio changes
233 due to coupled effects of roots growth and suction. The curve represents well the measurements for samples
234 in which a high root volumetric content was observed (i.e. R_v close to 0.007).

235 ## 3.2. Mechanical behaviour of the soil in tension

236 For the first stage of this study, tensile tests carried out at similar hydraulic states were compared. The stress-
237 displacement behaviour of the samples at low suction values is shown in Figure 7. As observed, vegetation
238 reinforces soil in tension, also at high saturation. Vegetated and non-vegetated soils follow the same
239 behaviour at very small displacements, indicating that the roots need to be stretched and aligned before
240 generating some reinforcement in the soil. Similar trends were observed in fibre-reinforced sands by Diambra
241 et al. (2010)[60], Tang et al. (2007)[61] and Heineck et al. (2005)[62], among others. Looking at the 27V and 28V
242 curves in the figure, the root area ratio *RAR* and the root length density R_{ld} measured in the bridge zone
243 complement soil reinforcement, resulting in a similar peak tensile strength of the composite material despite
244 the minor matric suction differences. A higher root length density makes the soil more ductile in the post-
245 peak phase, decreasing the rate of soil strength loss. The lower *RAR* (0.0010) observed in sample 21V
246 corresponds to 1-month growth vegetation (see Table 3) and already avoided an abrupt loss of strength,
247 compared to the fallow soil, even with no remarkable increase in the maximum stress. At the end of the tests
248 carried out within the abovementioned ranges of low matric suction, it was observed that the roots were
249 basically slipped and pulled out of the soil (i.e., without breaking at the point of the crack). This observation
250 will be mathematically formalised later in section 4.2. Hence, one can infer that the increase in soil strength
251 was mainly due to the tangential (friction) stresses developed throughout each soil-root interface in the
252 proximity of the cracking zone.

253 The combination of slightly drier hydraulic states (within the field capacity) and roots presence enhanced the
254 soil reinforcement effectiveness. Indeed, at matric suctions around 30-45 kPa, the vegetated soil exhibited
255 equal or higher tensile strengths than the corresponding fallow soil at s = 65 kPa (Figure 8-a). These
256 observations at the phenomenological scale may be correlated to the complex chemo-mechanical
257 interactions that occur at the microscale and the soil-root interface. As soil is drying, it shrinks around the
258 lateral roots kept attached to the mucilage matrix, embedding the roots firmly and generating a more robust
259 contact, which avoids roots slippage and pull-out. Indeed, during tests carried out at higher matric suction,
260 the roots mainly broke down, reaching their tensile strength. This effect is even more evident at suctions
261 higher than 100 kPa (Figure 8-b). In this case, the vegetated soil exhibited a stiffer response than the bare
262 soil at the beginning of the tests, jointly with a brittle behaviour, when the extended roots reached their
263 tensile strength. The unbroken roots ensured a residual soil strength in the post-peak behaviour (Figure 8-b).
264 In some cases, a further strength increase in the post-peak was clearly observed (sample 29V, Figure 8-b).
265 For example, the difference in tensile force between test 25V (vegetated) and test 5B (bare) is shown in
266 Figure 8-c. These two tests were chosen because they were conducted at similar matric suctions. Some drops
267 of around 3-4 N can be clearly observed, and these may be due to root breakage or natural vibrations
268 affecting the load cell. Such drops are equivalent to soil tensile stress decrease of 1.5-2 kPa (considering the
269 area of the soil bridge equal to 50·40 mm^2). After tensile strength peak, the residual resistance observed in
270 some vegetated soil samples (i.e. 25 kPa in 25V, Figure 8) is due to roots still stretching/slipping within the
271 soil matrix. In the case of sample 25V, it should be remarked that at displacements lower than 0.5 mm, 25
272 kPa of strength were already lost after the peak, indicating that at least 50% of roots broke down. Having
273 50% of broken roots with 80% of broken RAR_b indicated that the roots that remained unbroken were the
274 ones with smaller diameters (and higher tensile strength, see Figure 11a). Those roots were more flexible
275 and penetrated small voids more easily, so they needed more displacement to stretch thoroughly, slip and
276 finally break. During slipping, friction forces are developed. Even if the soil-root interface friction angle
277 remains the same (intrinsic property of the material), the confinement is considerably and isotropically
278 increasing with matric suction. This confinement, in turn, leads to increased frictional stresses at the soil root
279 interface, taking up a considerable part of the reinforcement.

4. MODELLING FRAMEWORK

4.1. Partially saturated soils

The tests have been furtherly interpreted within a shear failure criterion for partially saturated soils[63-65] with constitutive stress:

$$\sigma' = (\sigma - u_a) + S_r^{\alpha} s \quad (1)$$

where s is the soil matric suction, σ is the total stress, u_a = 0 is the relative atmospheric pressure and S_r^{α} is the effective degree of saturation representing the volume of water present in soil's macro-pores. The principal total stresses are:

$$\sigma_3 = \sigma_t \quad (2)$$

$$\sigma_1 = \sigma_2 = 0 \quad (3)$$

where σ_t is the tensile stress (negative, according to conventional geotechnical sign). The stress variables calculated at the peak tensile stress are represented in the *q-p'* invariants plane (*q* is the deviator stress and *p'* the mean skeleton stress):

$$q = \sigma_1 - \sigma_3 = -\sigma_t \quad (4)$$

$$p' = \frac{\sigma_1 + \sigma_2 + \sigma_3}{3} + S_r^{\alpha} s = \frac{\sigma_t}{3} + S_r^{\alpha} s \quad (5)$$

The Mohr-Coulomb extension-type failure criterion links the two stress variables:

$$q = \frac{6c' cos\varphi'}{3 + sin\varphi'} + M_e p' \quad (6)$$

where φ' is the friction angle and *c'* the cohesion at saturation, $M_e = 6sin\varphi'/(3+sin\varphi')$ is the slope of the failure envelope.

Three failure envelopes have been calibrated (Figure 9): one for fallow and two for vegetated soils. These last represent the plant's growth stages of 1 and 3 months and with average $RAR = A_{roots}/A_{soil}$ = 0.0012 and 0.0063, respectively. A_{roots} is the area of all the roots found within the soil crack, with area A_{soil}, generated by the test. In the case of multiple cracks, average values of A_{roots} and A_{soil} were considered. The model

297 parameters calibrated are listed in Table 4 for the three soils. At one month of plant growth, the vegetated
298 soil already presented an enhanced mechanical behaviour in terms of cohesion, which further increased at
299 three months (from 0 to 2.7 kPa at one month and 9.9 kPa at three months). In addition, some effects on the
300 friction angle were observed, with an increase of φ' from 2.9° (one month) to 4.9° (three months).

301 The shear strength parameters calibrated in this study are similar, in terms of φ' and c', to those obtained
302 with triaxial tests in the field capacity domain reported by Fraccica (2019)[12] on the same fallow and vegetated
303 soil with similar normalised roots quantities (φ'_{fallow} = 35.1°, c'_{fallow} = 0 kPa, φ'_{veg} = 36.6°, c'_{veg} = 10 kPa). Thus,
304 despite the detrimental effect of roots on soil hydraulic behaviour (an increase of void ratio/generation of
305 fissures due to roots' growth[51], and a decrease of S_r for a given matric suction s, see Figure 6), soil mechanical
306 properties were enhanced, within the range of matric suction investigated.

307 Although some change of the friction angle was detected, the higher impact of the vegetation was reflected
308 in an increase of cohesion and a decrease of the α parameter controlling the effective degree of saturation.
309 This last is linked to the changes in the hydraulic behaviour previously observed: roots generate macro-pores
310 and clog micro-pores as they grow in soil[12,55,66]. This change in soil structure is affecting the water retention
311 properties.

312 ## 4.2. Roots reinforcement model

313 Root reinforcement Δq_{roots} was evaluated as:

$$\Delta q_{roots} = q_{veg} - q_{fallow} \quad (7)$$

314 where q_{veg} is given by the peak results on the vegetated soil and q_{fallow} is the deviator stress evaluated on the
315 failure envelope for the same p'. As the onset of soil cracks was consistently observed in correspondence
316 with peak tensile stresses, these last values were chosen to interpret the root reinforcement. Thus, the
317 residual stresses were generated only by friction at the soil-root interfaces of unbroken roots when the soil
318 was already cracked.

319 The effect of the two main roots' failure mechanisms - root pull-out (mainly in nearly saturated samples) and
320 root breakage (in slightly saturated samples and within the field capacity) – on soil reinforcement at peak

conditions (just after the activation of roots stretching) was assessed. The fraction of the area of the broken roots to their total area found within the soil crack, RAR_b/RAR (also refer to Table 2), was defined to investigate the coupling between roots breakage and hydraulic state. In Figure 10, it is possible to detect a logarithmic increase of the ratio as a function of the hydraulic state, indicated by the product $S_r^{\alpha}s$. In nearly saturated soils (low $S_r^{\alpha}s$), most of the roots slipped out of the soil crack and a small fraction of them broke after a fixed tensile displacement (d = 1 mm). At the same displacement and higher $S_r^{\alpha}s$, the fraction of broken roots increased. This result suggests that root reinforcement is strongly affected by soil moisture and is in line with reported plant pull-out experiments[43,67]. However, due to the complexity and the number of variables linked to root's architecture, it is unsound to define a matric suction threshold that limits the occurrence of the two phenomena, whereas it is more likely that there is a transition range of matric suctions in which some roots are slipping and some other breaking at the same time. From Figure 7 and Figure 8, it is possible to infer that the maximum mobilisation of both soil-root friction and root tensile strength (breakage) occurs close to the peak, which is also close to the one detected in bare soil. Moreover, the short average length of the roots in the soil bridge (72.62 ± 20.32 mm, see Table 3) did not allow too much stretching before reaching pull-out or breakage in the plants. For these reasons, it was decided to sum the two equations governing roots reinforcement due to breakage and friction at the soil-root interface and to correlate them to the modelled deviator stress increase Δq_{roots}^{m} as:

$$\Delta q_{roots}^{m} = \Delta q_{breakage} + \Delta q_{friction} \quad (8)$$

where:

$$\Delta q_{breakage} = -\beta \sigma_{t,roots}\, RAR_b = -\beta \sigma_{t,roots}[0.14\, RAR \ln(1 + S_r^{\alpha}s) + 0.39] \quad (9)$$

The expression was adapted from the model of Wu et al. (1979)[39], in which the original correlation parameter β was calibrated through direct observations in landslides' scarps and through direct shear tests in saturated soils, and evaluated to be 1.2. $\sigma_{t,roots}$ (negative according to geotechnical sign) is the roots tensile strength and RAR_b (the broken roots' area ratio) substituted the originally proposed RAR. The evolution of RAR_b with the hydraulic state is presented in Figure 10 (see also Table 2). Root tensile strength evolution as a function of the root diameters is shown in Figure 11a. It is interesting to remark that root's strength diminishes as its

diameter increases. This behaviour is due to a higher fraction of lignin (a low resistant material) in thicker roots and a higher fraction of cellulose (high resistant material) in low-diameter roots[68]. Moreover, as the growing period increases (from one to three months in this study), the average diameter of the roots increases (Figure 11b and Table 3). Hence, the mean root diameter was calculated for each test and the mean root tensile strength accordingly to interpret the results.

The friction (pull-out) contribution to soil reinforcement is:

$$\Delta q_{friction} = \frac{n_{roots} f_d \left\{ [\tau_{soil-roots} \pi d_{roots} (l_{roots} - d)] + \left[\eta_b \frac{(l_{roots} - d)}{b_d} \right] \right\}}{A_{soil}} \quad (10)$$

The numerator has been proposed by Schwarz et al. (2010)[44] and represents the friction force that n_{roots} roots are opposing to slip-out after a tensile displacement d (considered herein as the displacement at which the peak tensile stress was observed). This value depends on the friction developed at the soil-root interface ($\tau_{soil-roots}$) and on the roots' branching distance (b_d). The parameters f_d and η_b are, respectively, a dynamic friction coefficient and a friction coefficient due to branching points. Indeed, Schwarz et al. (2010)[44] formalised that the closer is the branching distance on a given root, the higher is the pull-out force required to extract that root, as additional effort is required to break the branching contacts. Finally, l_{roots} is the average root length, d_{roots} is the average root diameter, and A_{soil} is the area of the soil crack. The values of the parameters of the roots used in Equations (9) and (10) are summarised in Table 3.

The soil-roots tangential stresses have been defined, in this study, as:

$$\tau_{soil-roots} = \tau_0 + \mu p' \quad (11)$$

in which τ_0 is the tangential stress that develops, due to soil grains-root interlocking and tortuosity effects, on the interface at saturated states. The term $\mu p'$ represents the tangential stress linked to the confinement exerted around the roots by the soil mean skeleton stress p', through the friction coefficient of the soil-root interface μ. According to Schwarz et al. (2010)[44], this last parameter depends mainly on soil physical properties (clay content, grain size distribution, soil plasticity). The choice to adopt the mean skeleton stress originates from the fact that roots present different orientations within the matrix and lie on multiple planes,

for which it is impossible to define a principal stress acting univocally on the soil-root interface. Moreover, this kind of stress variable allows including soil matric suction and degree of saturation at the same interface.

Once the parameters of the reinforcement equations were defined, the root properties found in the bridge of each sample (Table 3), jointly with *Sr* and *s*, were used as variables of the model. The predicted deviator stress in the vegetated samples $q_{model} = q_{fallow} + \Delta q^m_{roots}$ was defined to verify the performance of the models. The value of q_{fallow} is the one obtained with the Mohr-Coulomb failure envelope for bare soil, in correspondence with the mean skeleton stress of each vegetated test. Δq^m_{roots} is based on Equations (8) to (10). The model parameters were calibrated by minimising the squared error between q_{model} and q_{veg} and are listed in Table 5. Good model performance can be observed in Figure 12, in which q_{model} is presented versus q_{veg} (measured values in vegetated soil). P-values and standard errors of calibrated parameters were calculated, despite their high number compared to the limited number of tests. As a non-linear equation was used and some variables were multiplied and divided by each other, it was difficult to infer which are the best model parameters to use. The statistical analyses will be furtherly discussed.

5. DISCUSSION

Different processes contributed to the change in soil behaviour under tensile stresses. On the one hand, the drying process to which all specimens were subjected contributed to increase soil strength and brittleness. The void ratio decreased along drying compared to the values observed at saturation (Figure 5), remaining consistently higher in samples with vegetation for a given hydraulic state. The increase in mean effective stress produced by matric suction enhanced the bonding capacity[43,55] at the soil-root interface, reducing root slippage and resulting in a higher fraction of broken roots in the cracks. On the other hand, roots affected soil structure (i.e. void ratio increase), with consequences on the hydraulic behaviour and the correlated mechanical response[63-65]. Roots increased soil tensile strength thanks to two different mechanisms: root slippage and breakage. In the first mechanism, friction and relative displacements generated shear stresses at the soil-root interface, allowing a redistribution of deformations and stresses over a larger volume of soil, as detected by PIV analysis (see Figure 13). In the second mechanism, root tensile strength was mainly exploited, as the soil firmly bonded roots. The effect of soil moisture on root tensile strength was not

393 investigated here, as the majority of roots of this study were tested under field capacity conditions (maximum
394 matric suction s = 200 kPa and far below the permanent wilting point[70-72]).

395 As observed in the experimental results and as formalised in the models used, the effectiveness and
396 mechanisms of root reinforcement depend on the soil stress variables. To analyse the tensile tests in a unique
397 framework, two principal total stresses in the samples were assumed to be null, while the third one
398 corresponded to the tensile stress. PIV validated this assumption (see Figure 13), through which the
399 deformation fields were inferred on the soil surface. Arching effects, strain localisation around sub-angular
400 shapes or additional confinement due to the grip forces at the soil-moulds interface were not detected within
401 the two ends of each sample. Indeed, strain localisation was always observed within the soil bridge: a single
402 crack in the bare and slightly saturated vegetated soils, while multiple cracks were detected in nearly
403 saturated vegetated samples (Figure 13). Although some confining stresses developed in the partitions of soil
404 close to the equipment ends, these were not measured.

405 Considering the contribution to strength increase due to root slippage, the formulation proposed by Schwarz
406 et al. (2010)[44] was used in this study, assuming that the soil-root interface resistance was mobilised along
407 the entire length of the roots. Although stresses may develop along the so-called "loaded" portion of the
408 root, it is not straightforward to derive the length of this portion from macro-scale observations. This would
409 imply a complex correlation between the total displacement of the apparatus and the stiffness of the root,
410 similarly to what proposed by Waldron (1977)[73] . Indeed, different unknowns, such as root orientations and
411 tortuosity, would add further uncertainties and model parameters to calibrate. Only the root lengths
412 observed in the bridge partition were considered in the model to attenuate this potential modelling
413 weakness.

414 Given the necessity of "easy to use" analytical models, it was decided to adapt the Wu et al. (1979)[39]
415 formulation to consider root reinforcement due to root tensile strength/breakage. One limitation of this
416 model is that roots are assumed to break all at the same time, while this is actually not true. However, the
417 model may give good predictions if an adequate weighing parameter is used and if only the soil peak strength
418 is predicted. In this sense, the contribution of the *RAR* has to be read as an estimation of the maximum

419 available root strength: the higher is the *RAR*, the higher will be the number of roots that are resisting
420 shearing. Then, the parameter β will indicate the actual weight of this contribution among the overall soil
421 reinforcement. Not surprisingly, the mentioned parameter resulted much lower than 1.2 (i.e. 0.60), proposed
422 by the original model. This is because only the breakage contribution was considered in the latter, neglecting
423 the soil hydraulic state and friction at the soil-root interface.

424 Although the good prediction of the results, in terms of coefficient of determination R^2, some calibrated
425 parameters had high p-values (Table 5) and high standard errors, thus appearing to have low significance. It
426 is important to note that the number of vegetated tests (18) is still low to have a good statistical sampling,
427 but they are novel in literature. The parameters themselves were calibrated from laboratory tests for the
428 first time in this study, so comparisons with other values from the literature were not possible. Concerning
429 Equation (9), the parameter β calibrated (with good significance) was half of the one proposed by Wu et al.
430 (1979)[39], confirming the over-predictive performance of that model, as also observed by other authors[40-41].
431 Concerning Equation (11), the tangential stress at the soil-root interaction τ_0 resulted higher than zero,
432 meaning that roots' tortuosity and root-grains interlocking had an active role in generating stresses at the
433 interface and reinforcing the soil, even at saturated states. A good significance and a low standard error were
434 calculated for this parameter. The soil-root friction angle $tan^{-1}(\mu)$ may appear low, but one has to consider
435 that it controls shear stresses developing on each of a large number of soil-root interfaces (see the number
436 of roots n_{roots} in Table 3). Statistical analyses indicated a low significance of this parameter. Besides, a small
437 soil-root friction angle is in line with the slight increase of strength observed in nearly saturated vegetated
438 soil (i.e. 4-6 kPa), despite a large number of roots within the samples (see i.e. 21V, 27V or 28V, with
439 respectively 27, 48 and 55 roots in the bridge, Table 3). The observations made by PIV suggested that a large
440 number of roots was mobilised in nearly saturated samples. Indeed, more redistributed deformation fields
441 were observed with respect to what was detected in the bare soil (localised crack), as shown in Figure 13.
442 These observations hence are consistent with a low soil-root interface friction angle.

443 The calibrated dynamic friction coefficient f_d controls the displacement rate effect on soil-root friction[67]. To
444 the authors' best knowledge, no f_d parameter values are reported in the literature. Finally, a low value of the

445 η_b parameter indicates a negligible and poor significant effect of the fine root's branches for this type of
446 (quite young) plant. Indeed, even if branching points were quite frequent, the roots departing from them
447 were still fine, very short and flexible.

448 The use of the mentioned plants' indicators seems to work well in predicting soil behaviour along the
449 extension paths tested in this study, while they had been usually assessed under triaxial compression stress
450 paths or direct shear tests[12,39,40,69]. Therefore, more tests are needed to test the significance of the
451 parameters and validate the model.

452 6. CONCLUSIONS

453 This study presented laboratory results and root reinforcement interpretations on a vegetated and partially
454 saturated silty sand tested under direct uniaxial extension.

455 The observed soil mechanical behaviour in tension depended on the hydraulic state of the material: ductile
456 in nearly saturated conditions and brittle in slightly saturated conditions within the field capacity. Moreover,
457 vegetation enhanced soil tensile strength and made it more ductile in the post-peak response after roots
458 stretching. These results confirm the positive effect of vegetation in preventing soil cracking upon tension.

459 Different roots' failure mechanisms (slippage and breakage of roots) were observed by comparing vegetated
460 soil responses at low and high matric suctions and measuring several morpho-mechanical root traits within
461 the samples.

462 Tensile strength results were then interpreted with a shear strength failure criterion for partially saturated
463 soils. Shear strength parameters were consistent with those obtained by triaxial compression tests on the
464 same soil with similar root contents. This evidence indicated that a soil shear strength criterion could
465 successfully interpret tensile tests on soils and that the use of normalised root contents is helpful to compare
466 different geotechnical tests with different sample sizes.

467 Roots morphological and mechanical features were correlated to the soil tensile/shear strength increase by
468 adopting and combining two reinforcement models related to different root reinforcement mechanisms in a
469 unique equation and considering the soil's hydro-mechanical states. The models, so far used for vegetated

soils under different stress paths, were thus proven to work even under uniaxial extension successfully. Laboratory observations and interpretations also suggest that models that consider root breakage should not be decoupled from those considering root slippage/interface friction, as the two mechanisms co-occur during soil shearing/tensioning and are both affected by soil saturation and confinement, among other variables. Furthermore, this study allowed back-calculating soil-root interface mechanical properties, a piece of valuable information for numerical modelling analyses involving soil-roots interactions.

Further studies are needed to provide more results on this topic in such a way as to perform more accurate statistical analyses. Also, the effects of roots in the range of soil matric suction not investigated here (i.e. above 200 kPa), as well as the effect of root moisture on its tensile strength, need to be explored to corroborate the reinforcement model with other root contents, growth stages and/or vegetation species.

Acknowledgements

The authors wish to acknowledge the support of the European Commission via the Marie Skłodowska-Curie Innovative Training Networks (ITN-ETN) project TERRE 'Training Engineers and Researchers to Rethink geotechnical Engineering for a low carbon future' (H2020-MSCA-ITN-2015- 675762). Furthermore, Alessandro Fraccica wishes to thank Mercedes Sondon (Universitat Politècnica de Catalunya, UPC), Luis Gandarillas, Ylenia Bianchi, Ferran Parera (support with PIV software) and Stefano Collico (support with statistical analysis).

REFERENCES

1. Vardon, P.J. 'Climatic influence on geotechnical infrastructure: a review', Environmental Geotechnics., 2015; 2, 166–74. https://doi.org/10.1680/envgeo.13.00055
2. Cazzuffi, D., Cardile, G., Gioffrè, D. 'Geosynthetic Engineering and Vegetation Growth in Soil Reinforcement Applications.' Transportation Infrastructure Geotechnology, 2014; 1, 262 – 300. https://doi.org/10.1007/s40515-014-0016-1
3. Yildiz, A., Graf, F., Rickli, C. and Springman, S.M. 'Determination of the shearing behaviour of root-permeated soils with a large-scale direct shear apparatus', Catena, 2018;166, 98–113. https://doi.org/10.1016/j.catena.2018.03.022
4. Yildiz, A., Graf, F., Rickli, C. and Springman, S.M. 'Assessment of plant-induced suction and its effects on the shear strength of rooted soils. Proceedings of the Institution of Civil Engineers – Geotechnical Engineering, 2019; 172(6): 507–519. https://doi.org/10.1680/jgeen.18.00209
5. Gonzalez-Ollauri, A. and Mickovski, S. 'Plant-soil reinforcement response under different soil hydrological regimes', Geoderma, 2017;285, 141–50. https://doi.org/10.1016/j.geoderma.2016.10.002
6. Fan, C. and Su, C.. Role of roots in the shear strength of root-reinforced soils with high moisture content. Ecological Engineering, 2008; 33(2):157–166. https://doi.org/10.1016/j.ecoleng.2008.02.013
7. Comino, E., Marengo, P. and Rolli, V. 'Root reinforcement effect of different grass species: A comparison between experimental and models results.' Soil & Tillage Research, 2010; 110(1):60–68. https://doi.org/10.1016/j.still.2010.06.006
8. Zhang, C.B., Chen, L.H., Liu, Y.P., Ji, X.D. and Liu, X.P. 'Triaxial compression test of soil-root composites to evaluate influence of roots on soil shear strength', Ecological Engineering, 2010; 36(1), 19–26. https://doi.org/10.1016/j.ecoleng.2009.09.005
9. Li, Y., Wang, Y., Wang, Y., Ma, C. 'Effects of root spatial distribution on the elastic-plastic properties of soil-root blocks'. Scientific Reports, 2017; 7, 800. https://doi.org/10.1038/s41598-017-00924-z
10. Ji, X. 'GDS Triaxial Test on the Reinforcement Effects of Bermudagrass Root-soil Complex', in IOP Conference Series: Earth and Environmental Science, 2019; 304, 032106. https://doi.org/10.1088/1755-1315/304/3/032106
11. Karimzadeh, A.A., Leung, A.K., Hosseinpour, S., Wu, Z., Amini, P.F. 'Monotonic and cyclic behaviour of root-reinforced sand'. Canadian Geotechnical Journal, 2021. Just-IN https://doi.org/10.1139/cgj-2020-0626
12. Fraccica, A. 'Experimental Study and Numerical Modelling of Soil-Roots Hydro-Mechanical Interactions', Universitat Politècnica de Catalunya; Université de Montpellier, 2019; PhD Thesis. https://hal.inrae.fr/tel-03109049
13. Meijer, G.J., Bengough, A.G., Knappett, J.A., Loades, K.W. and Nicoll, B.C. 'New in-situ techniques for measuring the properties of root-reinforced soil – Laboratory evaluation.' Géotechnique, 2016; 66(1), 27–40. https://doi.org/10.1680/jgeot.15.P.060
14. Meijer, G.J., Bengough, A.G., Knappett, J.A., Loades, K.W. and Nicoll, B.C. 'In situ measurement of root reinforcement using corkscrew extraction method.' Canadian Geotechnical Journal, 2018; 55(10), 1372-1390. https://doi.org/10.1139/cgj-2017-0344
15. Chen, G., Zheng, S., Zhu, J., Wang, W. and Feng, W. 'A quantitative display index that considers tensile failure to predict the full sliding surface of a landslide', Landslides, 2020; 17, 471–482. https://doi.org/10.1007/s10346-019-01301-9
16. Potts, D.M. and Zdravkovic, L. 'Finite Element Analysis in Geotechnical Engineering: Theory' Published by Thomas Telford Publishing, Thomas Telford Ltd, 1 Heron Quay, London EI44JD, 1999. ISBN: 0 7277 2753 2

17. Cui, Y.J. and Delage, P. 'Yielding and plastic behaviour of an unsaturated compacted silt', Géotechnique, 1996; 46(2), 291–311. https://doi.org/10.1680/geot.1996.46.2.291
18. Kuwano, R. 'The stiffness and yielding anisotropy of sand', Imperial College of Science, Technology and Medicine, 1999, PhD Thesis. http://geo.iis.u-tokyo.ac.jp/member/documents/PhDKuwano1999.pdf
19. Yasufuku, N., Murata, H. and Hyodo, M. 'Yield Characteristics of Anisotropically Consolidated Sand Under Low and High Stresses', Soils and Foundations, 1991; 31(1), 95–109. https://doi.org/10.3208/sandf1972.31.95
20. Alonso, E.E., Gens, A. and Delahaye, C.H. 'Influence of rainfall on the deformation and stability of a slope in overconsolidated clays: a case study', Hydrogeology Journal, 2003; 11, 174–92 https://doi.org/10.1007/s10040-002-0245-1
21. Kodikara J., Costa S. 'Desiccation Cracking in Clayey Soils: Mechanisms and Modelling'. In: Laloui L., Ferrari A. (eds) Multiphysical Testing of Soils and Shales, 2013. Springer Series in Geomechanics and Geoengineering. Springer, Berlin, Heidelberg. https://doi.org/10.1007/978-3-642-32492-5_2
22. Yanamandra, G., Oh, W.T. 'Influence of Excavation Time, Tension Crack, and Rainfall on the Stability of Unsupported Vertical Cuts in Unsaturated Soil', International Journal of Geomechanics, 2021; 21(10), 04021199 https://doi.org/10.1061/(ASCE)GM.1943-5622.0002160
23. Luo, Y., Zhang, J. M., Zhou, Z., Shen, Z. J., Chong, L., Victor, C. 'Investigation and prediction of water infiltration process in cracked soils based on a full-scale model test'. Geoderma, 2021, 400, 115111. https://doi.org/10.1016/j.geoderma.2021.115111
24. Zeng, L., Xiao, L. Y., Zhang, J. H., Gao, Q. F. 'Effect of the characteristics of surface cracks on the transient saturated zones in colluvial soil slopes during rainfall'. Bulletin of Engineering Geology and the Environment, 2020, 79(2), 699-709. https://doi.org/10.1007/s10064-019-01584-1
25. Cotecchia F, Vitone C, Santaloia F, Pedone G, Bottiglieri O. 'Slope instability processes in intensely fissured clays: case histories in the southern Apennines'. Landslides, 2015 12(5), 877–893 https://doi.org/10.1007/s10346-014-0516-7
26. Arnold, J.G., Potter, K.N., King, K.W. and Allen, P.M. 'Estimation of soil cracking and the effect on surface runoff in a Texas Blackland Prairie watershed', Hydrological Processes, 2005; 19, 589–603. https://doi.org/10.1002/hyp.5609
27. Lakshmikantha, M.R., Prat, P.C. and Ledesma, A. 'Experimental evidence of size effect in soil cracking', Canadian Geotechnical Journal, 2012; 49(3), 264–284. https://doi.org/10.1139/t11-102
28. Cordero, J., Najdi, A., Encalada, D., Prat, P.C., Ledesma, A. 'Experimental and numerical analysis of soil desiccating cracks in compacted and non-compacted specimens'. in R. Cardoso, C. Jommi and E. Romero (eds), 4th European Conference on Unsaturated Soils - E-UNSAT2020. E3S Web of Conferences, 2020; 195, 03021. https://doi.org/10.1051/e3sconf/202019503021
29. Stirling, R.A., Hughes, P., Davie, C.T. and Glendinning, S. 'Tensile behaviour of unsaturated compacted clay soils - A direct assessment method', Applied Clay Science, 2015; 112–113, 123–133. http://dx.doi.org/10.1016/j.clay.2015.04.011
30. Murray, I. and Tarantino, A. 'Mechanisms of failure in saturated and unsaturated clayey geomaterials subjected to (total) tensile stress', Géotechnique, 2019; 69(8), 701–712. https://doi.org/10.1680/jgeot.17.P.252
31. Trabelsi, H.; Romero, E.; Jamei, M. 'Tensile strength during drying of remoulded and compacted clay: the role of fabric and water retention.' Applied Clay Science 2018; 162, 57-68. https://doi.org/10.1016/j.clay.2018.05.032
32. Divya, P. V, Viswanadham, B.V.S. and Gourc, J.P. 'Evaluation of Tensile Strength-Strain Characteristics of Fiber-Reinforced Soil through Laboratory Tests', Journal of Materials in Civil Engineering, 2014; 26(1), 14–23. https://doi.org/10.1061/(ASCE)MT.1943-5533.0000772
33. Trabelsi, H., Chebbi, M., Guiras, H., Jamei, M. and Romero, E. 'Stabilization of clayey soil using fiber reinforcement', in The 7th International Conference on Unsaturated Soils, UNSAT2018 (Hong Kong:

586 The Hong Kong University of Science and Technology (HKUST)), 2018; 545–550.
587 http://hdl.handle.net/2117/129409
588 34. Consoli, N.C., de Moraes, R.R., Festugato, L. 'Split tensile strength of monofilament polypropylene
589 fiber-reinforced cemented sandy soils.' Geosynthetics International, 2011; 18 (2), 57–62.
590 https://doi.org/10.1680/gein.2011.18.2.57
591 35. Bordoloi, S., Gadi, V.K., Hussain, R., Sahoo, L., Garg, A., Sreedeep, S., Mei, G., Poulsen, T.G. 'Influence
592 of *Eichhornia crassipes* fibre on water retention and cracking on vegetated soils'. Géotechnique
593 Letters, 2018; 8(2), 130 – 137. https://doi.org/10.1680/jgele.17.00181
594 36. Bordoloi, S., Ni, J., Ng, C.W.W. 'Soil desiccation cracking and its characterization in vegetated soil: A
595 perspective review. Science of the Total Environment, 2020; 729, 138760.
596 https://doi.org/10.1016/j.scitotenv.2020.138760
597 37. Li, J.H., Li, L., Chen, R., Li, D.Q. 'Cracking and vertical preferential flow through landfill clay liners.'
598 Engineering Geology, 2016; 206, 33 – 41. https://doi.org/10.1016/j.enggeo.2016.03.006
599 38. Fraccica, A., Romero, E., Fourcaud, T., Sondon, M. and Gandarillas, L. 'Tensile strength of a vegetated
600 and partially saturated soil', in R. Cardoso, C. Jommi and E. Romero (eds), 4th European Conference
601 on Unsaturated Soils - E-UNSAT2020. E3S Web of Conferences, 2020; 195, 03001.
602 https://doi.org/10.1051/e3sconf/202019503001
603 39. Wu, T.H., McKinnell III, W.P. and Swanston, D.N. 'Strength of tree roots and landslides on Prince of
604 Wales Island, Alaska', Canadian Geotechnical Journal, 1979; 16(1), 19–33.
605 https://doi.org/10.1139/t79-003
606 40. Mickovski, S., Hallett, P.D., Bransby, M.F., Davies, M.C.R., Sonnenberg, R. and Bengough, A.G.
607 'Mechanical Reinforcement of Soil by Willow Roots: Impacts of Root Properties and Root Failure
608 Mechanism', Soil Science Society of America Journal, 2009; 73, 1276–1285.
609 https://doi.org/10.2136/sssaj2008.0172
610 41. Pollen, N. and Simon, A. 'Estimating the mechanical effects of riparian vegetation on stream bank
611 stability using a fiber bundle model', Water Resources Research, 2005; 41, W07025.
612 https://doi.org/10.1029/2004WR003801
613 42. Coppin, N.J. and Richards, I.G. 'Use of Vegetation in Civil Engineering', 1st Ed. London: CIRIA
614 Butterworths, 1990. ISBN: 0-408-03849-7
615 43. Pollen, N. 'Temporal and spatial variability in root reinforcement of streambanks: Accounting for soil
616 shear strength and moisture', Catena, 2007; 69(3), 197–205.
617 https://doi.org/10.1016/j.catena.2006.05.004
618 44. Schwarz, M., Lehmann, P. and Or, D. 'Quantifying lateral root reinforcement in steep slopes - from a
619 bundle of roots to tree stands', Earth Surface Processes and Landforms, 2010; 35, 354–367.
620 https://doi.org/10.1002/esp.1927
621 45. Weng, Z., Wang, J., Senthil, T., Wu, L. 'Mechanical and thermal properties of ABS/montmorillonite
622 nanocomposites for fused deposition modeling 3D printing.' Materials and Design, 2016; 102, 276-
623 283. http://dx.doi.org/10.1016/j.matdes.2016.04.045
624 46. Interstate Plastic Inc. (2019). https://www.interstateplastics.com/ABS-sheets-rods
625 47. ASTM D3080 / D3080M (2011) 'Standard Test Method for Direct Shear Test of Soils Under
626 Consolidated Drained Conditions', ASTM International, West Conshohocken, PA, 2011 [Online]
627 Available at: www.astm.org
628 48. Nahlawi, H., Chakrabarti, S., and Kodikara, J. 'A Direct Tensile Strength Testing Method for
629 Unsaturated Geomaterials' Geotechnical Testing Journal, 2004; 27(4), 356-361.
630 https://doi.org/10.1520/GTJ11767
631 49. Oorthuis, R., Hürlimann, M., Fraccica, A., Lloret, A., Moya, J., Puig-Polo, C. and Vaunat, J. 'Monitoring
632 of a full-scale embankment experiment regarding soil-vegetation-atmosphere interactions', Water
633 (Switzerland), 2018; 10(6), 688. https://doi.org/10.3390/w10060688

50. Oorthuis, R., Vaunat, J., Hürlimann, M., Lloret, A., Moya, J., Puig-Polo, C. and Fraccica, A. 'Slope Orientation and Vegetation Effects on Soil Thermo-Hydraulic Behavior'. An Experimental Study. Sustainability, 2021; 13(1), 14. https://doi.org/10.3390/su13010014
51. Fraccica, A., Romero, E. and Fourcaud, T. 'Multi-scale effects on the hydraulic behaviour of a root-permeated and compacted soil', in A. Tarantino and E. Ibraim (eds), IS-Glasgow (Glasgow), E3S Web of Conferences, 2019; 92, 12014 https://doi.org/10.1051/e3sconf/20199212014
52. ASTM D2216 (2019) 'Standard Test Methods for Laboratory Determination of Water (Moisture) Content of Soil and Rock by Mass' [Online] Available at: www.astm.org
53. ASTM D7263 (2018) 'Standard Test Method for Laboratory Determination of Density (Unit Weigth) of Soil Specimens.' [Online] Available at: www.astm.org
54. Muir Wood, D., Diambra, A., Ibraim, E.. 'Fibres and soils: A route towards modelling of root-soil systems'. Soils and Foundations, 2016; 56(5), 765-778. https://doi.org/10.1016/j.sandf.2016.08.003
55. Carminati, A., Vetterlein, D., Koebernick, N., Blaser, S., Weller, U. and Vogel, H.J. 'Do roots mind the gap?', Plant and Soil, 2013; 367, 651–661. https://doi.org/10.1007/s11104-012-1496-9
56. Ni, J., Sanandam, B., Garg, A., Shao, W., and Sreedeep, S. 'Simple Model on Water Retention and Permeability in Soil Mixed with Lignocellulose Fibres.' KSCE Journal of Civil Engineering, 2019; 23, 138–146. https://doi.org/10.1007/s12205-017-0657-z
57. Ng, C.W.W., Leung, A.K. and Woon, K.X. 'Effects of soil density on grass-induced suction distributions in compacted soil subjected to rainfall', Canadian Geotechnical Journal, 2014; 51(3), 311–321. https://doi.org/10.1139/cgj-2013-0221
58. Romero, E., and Vaunat, J. 'Retention curves of deformable clays.' Experimental Evidence and Theoretical Approaches in Unsaturated Soils, Tarantino A. and Mancuso C. (eds). CRC Press, 2000. 99-114. https://doi.org/10.1201/9781482283761
59. Romero, E., Della Vecchia, G., and Jommi, C. An insight into the water retention properties of compacted clayey soils. Géotechnique, 2011; 61(4), 313-328. https://doi.org/10.1680/geot.2011.61.4.313
60. Diambra, A., Ibraim, E., Muir Wood, D. and Russell, A. R. 'Fibre reinforced sands: Experiments and modelling.' Geotextiles and Geomembranes, 2010; 28(3):238–250. https://doi.org/10.1016/j.geotexmem.2009.09.010
61. Tang, C., Shi, B., Gao, W., Chen, F. and Cai, Y. 'Strength and mechanical behavior of short polypropylene fiber reinforced and cement stabilized clayey soil.' Geotextiles and Geomembranes, 2007; 25(3):194–202. DOI: 10.1016/j.geotexmem.2006.11.002
62. Heineck, K. S., Coop, M. R. and Consoli, N. C. 'Effect of microreinforcement of soils from very small to large shear strains.' Journal of Geotechnical and Geoenvironmental Engineering, 2005; 131(8):1024–1033. https://doi.org/10.1061/(ASCE)1090-0241(2005)131:8(1024)
63. Vanapalli, S. K., Fredlund, D. G., Pufahl, D. E. and Clifton, A. W.' Model for the prediction of shear strength with respect to soil suction'. Canadian Geotechnical Journal, 1996;33(3), 379–392. https://doi.org/10.1139/t96-060
64. Tarantino, A. and Tombolato, S.. 'Coupling of hydraulic and mechanical behaviour in unsaturated compacted clay'. Géotechnique, 2005; 55(4), 307–317. https://doi.org/10.1680/geot.2005.55.4.307
65. Alonso, E.E., Pereira, J.M., Vaunat, J. and Olivella, S. 'A microstructurally based effective stress for unsaturated soils', Géotechnique, 2010; 60(12), 913–925. https://doi.org/10.1680/geot.8.P.002
66. Scholl, P., Leitner, D., Kammerer, G., Loiskandl, W., Kaul, H.P. and Bodner, G. 'Root induced changes of effective 1D hydraulic properties in a soil column', Plant and Soil, 2014; 381, 193–213. https://doi.org/10.1007/s11104-014-2121-x
67. Mickovski, S.B., Bengough, A.G., Bransby, M.F., Davies, M.C.R., Hallett, P.D. and Sonnenberg, R. 'Material stiffness, branching pattern and soil matric potential affect the pullout resistance of model root systems', European Journal of Soil Science, 2007; 58, 1471–1481. https://doi.org/10.1111/j.1365-2389.2007.00953.x

68. Genet, M., Stokes, A., Salin, F., Mickovski, S.B., Fourcaud, T., Dumail, J.F., et al. 'The influence of cellulose content on tensile strength in tree roots'. In: Stokes A., Spanos I., Norris J.E., Cammeraat E. (eds) Eco-and Ground Bio-Engineering: The Use of Vegetation to Improve Slope Stability. Developments in Plant and Soil Sciences, vol 103. Springer, Dordrecht. https://doi.org/10.1007/978-1-4020-5593-5_1
69. Tardío, G. and Mickovski, S.B. 'Method for synchronisation of soil and root behaviour for assessment of stability of vegetated slopes', Ecological Engineering, 2015; 82, 222–230. https://doi.org/10.1016/j.ecoleng.2015.04.101
70. Li, L., Young, J., and Deb, S. 'Effects of cultivation practices and products on bermudagrass fairways in a semiarid region.' Agronomy Journal, 2019; 111(6), 2899-2909. https://doi.org/10.2134/agronj2019.04.0262
71. Bochet, E., and García-Fayos, P. 'Factors controlling vegetation establishment and water erosion on motorway slopes in Valencia, Spain.' Restoration Ecology, 2004; 12(2), 166-174. https://doi.org/10.1111/j.1061-2971.2004.0325.x
72. de Abelleyra, D., Verdu, A. M. C., Kruk, B. C., and Satorre, E. H. 'Soil water availability affects green 'area and biomass growth of Cynodon dactylon.' Weed research, 2008; 48(3), 248-256. https://doi.org/10.1111/j.1365-3180.2008.00624.x
73. Waldron, L.J. 'The shear resistence of root-permeated homogeneous and stratified soil.' Soil Science Society of America Journal, 1977; 41, 843–849 https://doi.org/10.2136/sssaj1977.03615995004100050005x

705 *Table 1 Soil physical properties*

Soil property	Value
Gravel fraction (%) > 2 mm	41.2[a]
75 μm < Sand fraction (%) < 2mm	28.0[a]
2 μm < Silt fraction (%) < 75 μm	25.4[a]
Clay fraction (%) < 2 μm	5.4[a]
Liquid limit (%)	29.5[b]-34.4[a]
Plasticity index (%)	9.6[b]-13.5[a]
Density of solids, ρ_s (Mg/m^3)	2.65[b]-2.70[a]

706 [a] Oorthuis et al. (2018)
707 [b] Fraccica et al. (2019)
708

Table 2 Roots' morpho-mechanical traits assessed in this study and their definitions

Name and formula	Description	Measurement method in this study
Average root diameter, d_{roots}	Average of the diameters of the roots observed in the soil partition	Calliper (resolution 0.02 mm)
Average root length, l_{roots}	Average of the lengths of the roots observed in the soil partition	Calliper (resolution 0.02 mm)
Branching point distance, b_d	Average distance between two branches on a given root	Calliper (resolution 0.02 mm)
Number of roots, n_{roots}	Number of roots found in each soil partition	Visual inspection
Root area ratio, $RAR = \Sigma_i A_{roots,i} / A_{soil}$	Area of all the roots in the crack divided by the crack soil surface	Calliper (resolution 0.02 mm)
Broken root area ratio, $RAR_b = \Sigma_i A_{b,roots,i} / A_{soil}$	Area of the broken roots in the crack (between 0 and 1 mm of tensile displacement) divided by the crack soil surface	Calliper (resolution 0.02 mm)
Root volume ratio, $R_v = V_{roots}/V_s$	Volume of roots normalised by the volume of solid particles in which it was found	Pycnometry (resolution 10 mm^3)
Root length density, $R_{ld} = \Sigma_i l_{roots,i} / V_s$	Sum of all the roots' lengths normalized by the volume of the solid particles in which it was found	Calliper (resolution 0.02 mm)
Roots tensile strength, $\sigma_{t,\,roots} = 12.5e^{(-2.4d_{roots})}$ **	Tensile strength of roots, evaluated in correspondence of the average root diameter	Tensile test on roots (resolution 0.003 N)

**Fraccica (2019)

Table 3 Soil tensile strength and hydraulic state and roots features in the bridge of the tested samples.

Sample # (months of growth)	Soil tensile strength, σ_t (kPa)	Average matric suction, s (kPa)	$S_r^{\alpha}s$ (kPa)	Average root diameter, d_{roots} (mm)	Average root length, l_{roots} (mm)	Average branching point distance, b_d (mm)	Number of roots, n_{roots} (-)	Root area ratio RAR and (RAR_b/RAR) (-)	Root volume ratio, R_v (-)	Root length density, R_{ld} (m/m^3)
VA(1)	- 3.1	9	1.8	0.52±0.13	89.52±16.2	2.60±0.6	46	0.0020 (0.50)	0.002	7.0 10^3
VB(1)	- 9.0	94	10.9	0.46±0.10	71.54±13.5	1.90±0.8	110	0.0022 (0.95)	0.007	1.1 10^4
VC(1)	- 3.6	17	2.6	0.45±0.12	52.64±11.5	1.88±0.7	72	0.0009 (0.64)	0.006	7.6 10^3
VD(1)	- 7.3	40	3.0	0.57±0.16	56.12±17.2	3.24±1.3	66	0.0010 (0.90)	0.007	1.1 10^4
VF(1)	- 3.4	11	2.2	0.51±0.20	67.56±20.1	1.77±1.5	91	0.0016 (0.56)	0.008	8.4 10^3
VG(1)	- 19.3	180	21.7	0.69±0.11	69.32±22.5	4.31±1.1	62	0.0057 (0.84)	0.002	3.8 10^3
VH(3)	- 18.3	200	11.4	0.84±0.14	56.92+15.2	5.94±0.8	152	0.0049 (0.77)	0.013	2.2 10^4
VI(3)	- 24.5	150	18.6	0.67±0.09	65.06±25.2	4.10±0.9	81	0.0040 (0.63)	0.007	1.2 10^4
V19(1)	- 1.4	1	0.3	0.40±0.11	57.2±17.2	1.18±0.6	45	0.0007 (0.40)	0.002	8.2 10^3
V20(1)	- 12.3	17	7.8	0.38±0.15	83.74±23.1	1.20±0.9	42	0.0009 (0.62)	0.002	1.1 10^4
V21(1)	- 6.0	3	0.9	0.42±0.22	78.8±28.1	1.14±0.7	27	0.0007 (0.44)	0.001	6.8 10^3
V22(1)	- 18.1	65	19.5	0.40±0.25	85.6±16.5	1.22±1.3	36	0.0009 (0.84)	0.002	9.8 10^3
V24(3)	- 27.4	45	25.0	0.50±0.26	56.94±18.1	2.55±1.0	60	0.0054 (0.88)	0.009	1.0 10^4
V25(3)	- 50.0	99	46.6	0.53±0.16	77.75±28.2	2.61±1.3	65	0.0081 (0.93)	0.014	1.4 10^4
V26(3)	- 22.0	29	17.5	0.54±0.14	93.43±32.5	2.58±0.9	30	0.0085 (0.81)	0.015	7.4 10^3
V27(3)	- 9.8	4	2.2	0.56±0.32	83.1±27.1	2.57±0.7	48	0.0093 (0.38)	0.018	7.5 10^3
V28(3)	- 10.0	1	0.6	0.50±0.27	79.46±18.7	2.63±0.9	55	0.0052 (0.36)	0.009	1.2 10^4
V29(3)	- 44.9	190	51.2	0.53±0.21	82.46±14.9	2.52±1.4	60	0.0054 (0.85)	0.010	1.2 10^3

Table 4 Failure envelope parameters calibrated in this study

Soil	α **(-)**	M_e **(-)**	c' **(kPa)**	φ' **(°)**
Silty sand	5.00	0.90	0.0	32.0
Silty sand + *Cynodon dactilon* (1 month of growth)	3.92	0.96	2.7	34.9
Silty sand + *Cynodon dactilon* (3 months of growth)	2.15	1.00	9.9	36.9

Table 5 Root-reinforcement model's parameters calibrated in this study, p-values and standard error of the regression's parameters (SE)

Parameter and symbol	**Value**	**p-values**	**SE**
Correlation parameter, β *(-)*	0.60	$2.19 \cdot 10^{-3}$	0.16
Dynamic friction coefficient, f_d *(-)*	0.37	$0.40 \cdot 10^{0}$	0.43
Branching friction coefficient, η_b *(kN)*	$1.52 \cdot 10^{-6}$	$0.80 \cdot 10^{0}$	$5.93 \cdot 10^{-6}$
Soil-root tangential stress at saturation, τ_0 *(kPa)*	0.90	$0.18 \cdot 10^{-3}$	0.18
Soil-root interface friction coefficient, μ (-)	0.02	$0.86 \cdot 10^{0}$	0.11
Soil-root interface friction angle, $tan^{-1}(\mu)$ (°)	1.23	-	-

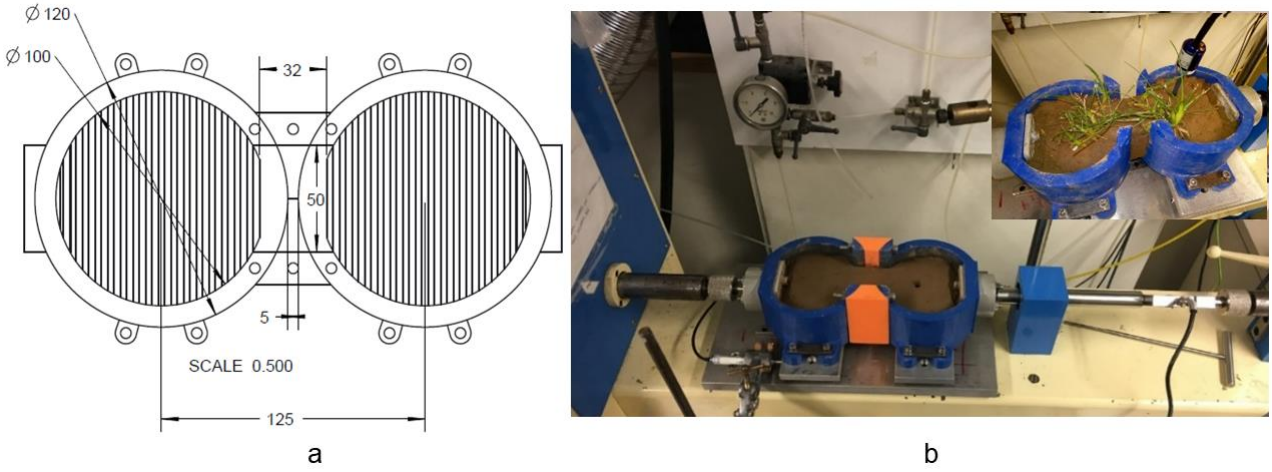

Figure 1 a) Plan view and dimensions of the equipment. B) In the large picture it is shown the setup prior to perform the tensile test, with the moulds connected to the load cell (right), to the motor and the horizontal LVDT (left). In the small picture the tensiometer installed in the specimen and the L-shaped orange pieces removed are shown.

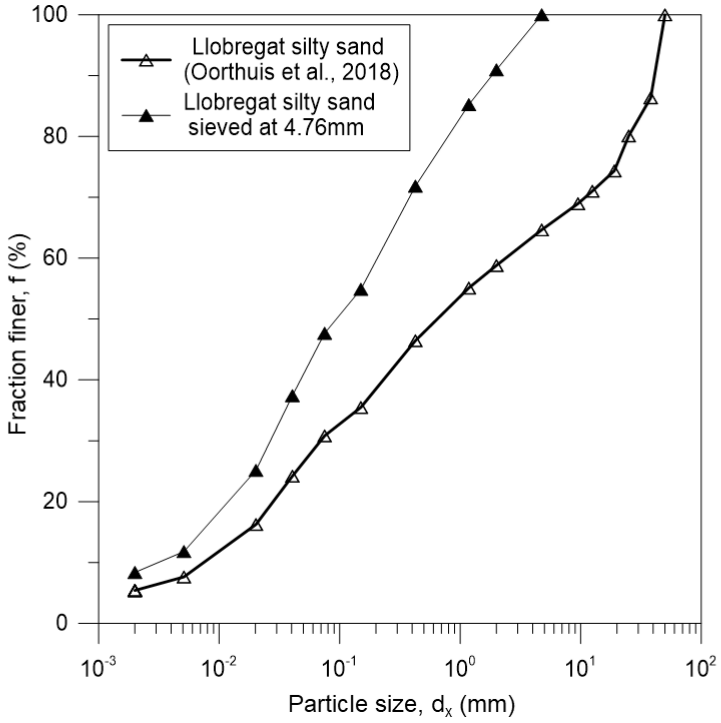

Figure 2 Grain size distribution of the original and sieved soil used in this investigation

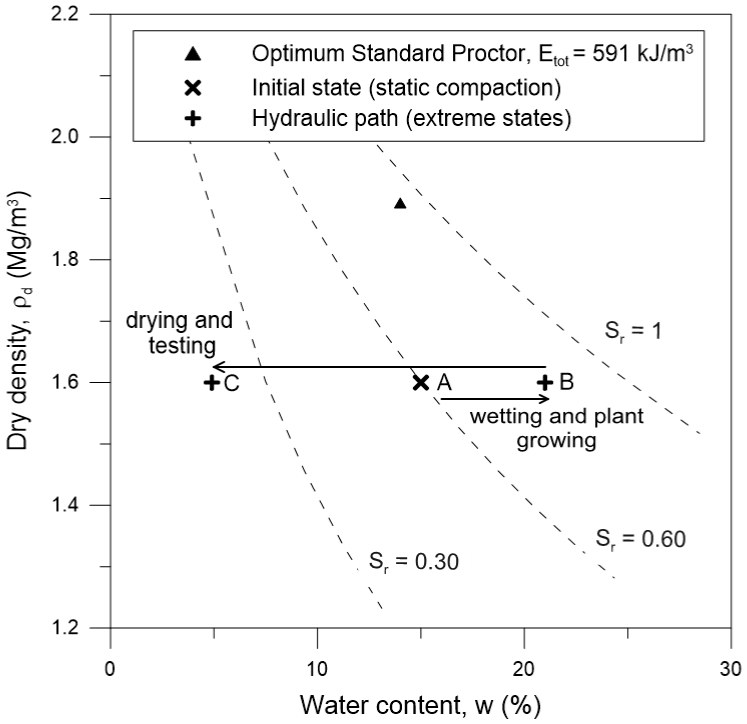

Figure 3 Hydraulic path imposed to the samples, prior to perform tensile tests.

a b

c d e

Figure 4 a) Identification of the three soil partitions within which root traits have been assessed separately. B) Root diameters measurements with calliper within the tensile crack. C) plant roots after retrieval (soil washing), d) measurement of root length and branching distance with the calliper, e) measurement of root volume with the pycnometer.

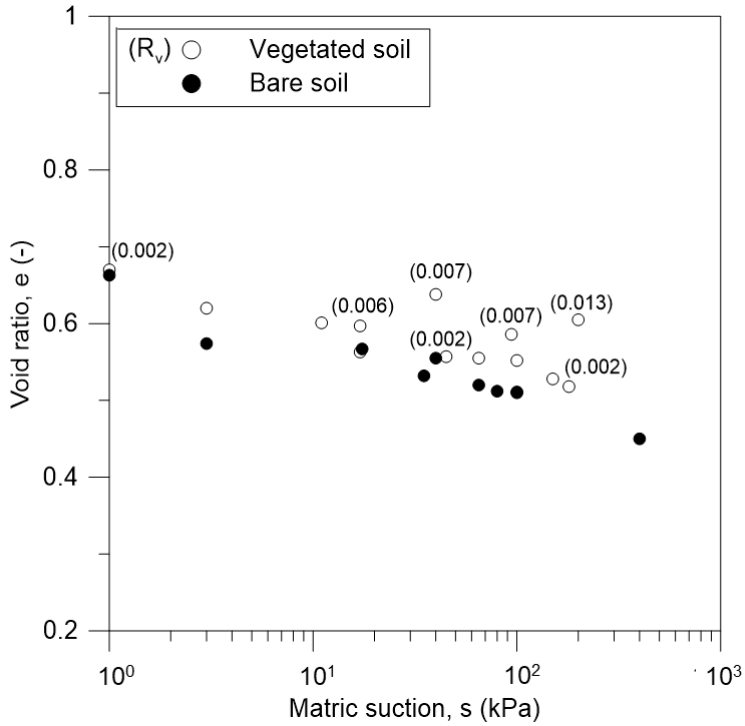

Figure 5 Void ratio evolution along the drying path imposed prior to perform soil tensile tests. Root volume ratio indicated as labels

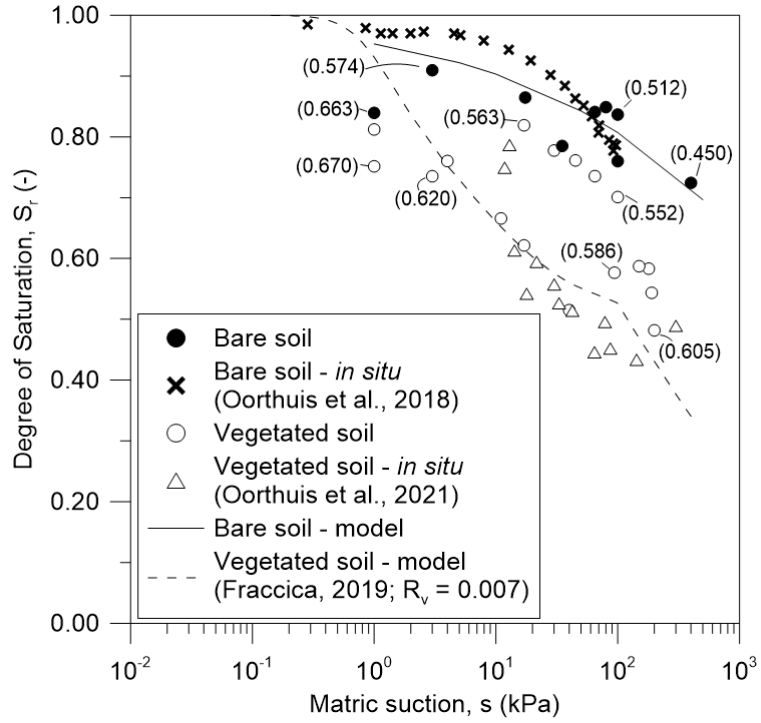

Figure 6 Retention behaviour of bare and vegetated soil. Comparison with bare (Oorthuis et al., 2018) and vegetated soil (embankment partition: SV – 16 cm, extracted from Oorthuis et al., 2021) of the in-situ full-scale experiment. Bare soil fitted with SWRC law proposed by Romero and Vaunat, 2000. Vegetated soil model produced by Fraccica, 2019, for vegetated soil samples with R_v = 0.007. Void ratio indicated as labels

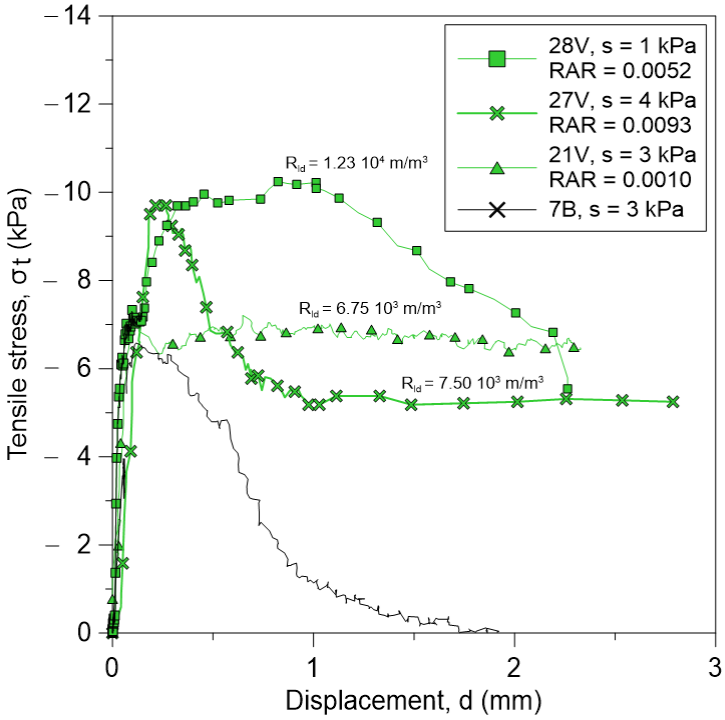

Figure 7 Comparison of direct tensile tests on bare and vegetated soil at low suction

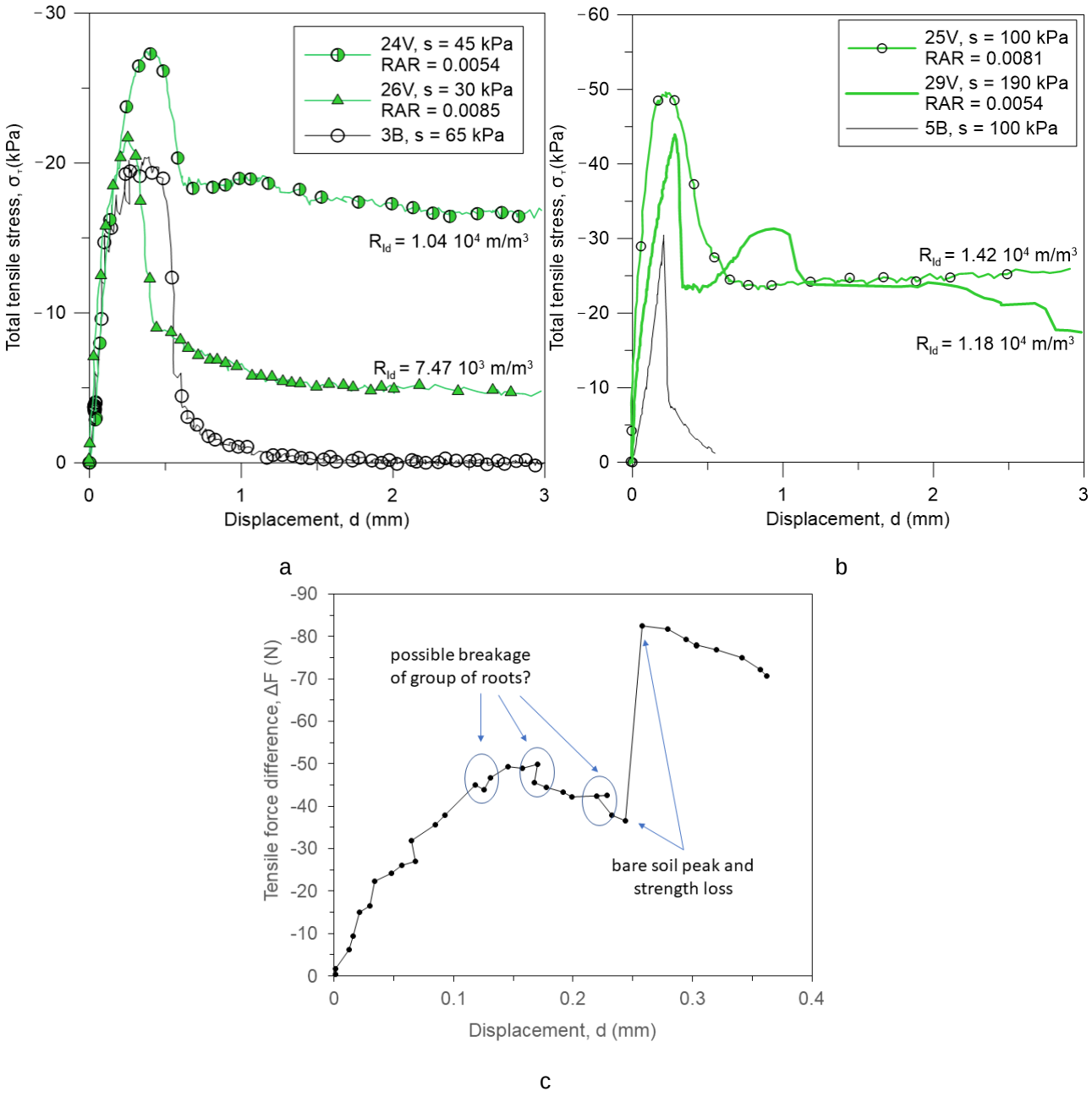

Figure 8 Comparison of direct tensile tests on bare and vegetated soil at high suction values: a) between 30 and 65 kPa, b) between 100 and 190 kPa. In c) the tensile force difference between tests 25V and 5B is represented

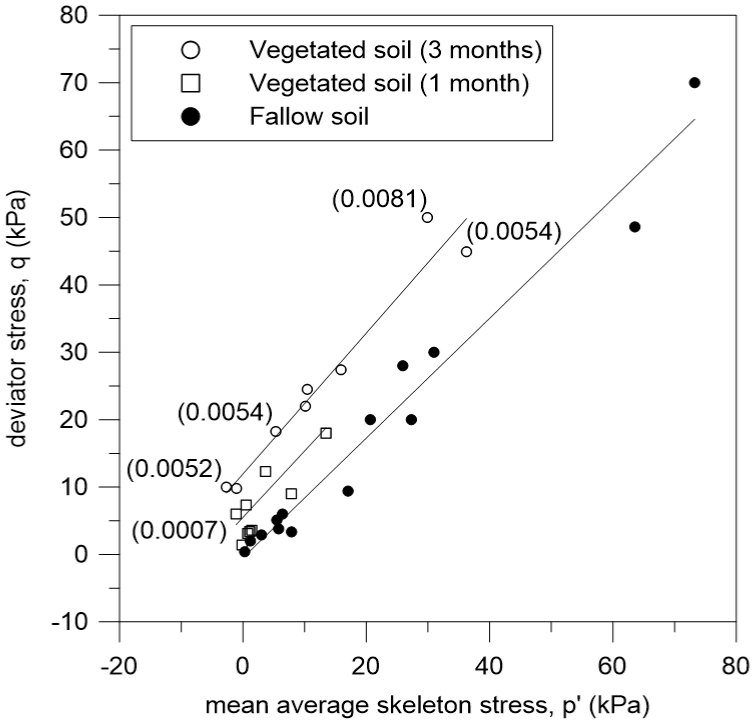

Figure 9 Failure envelopes for the bare and the vegetated soil at two plants' growth stages. RAR as labels

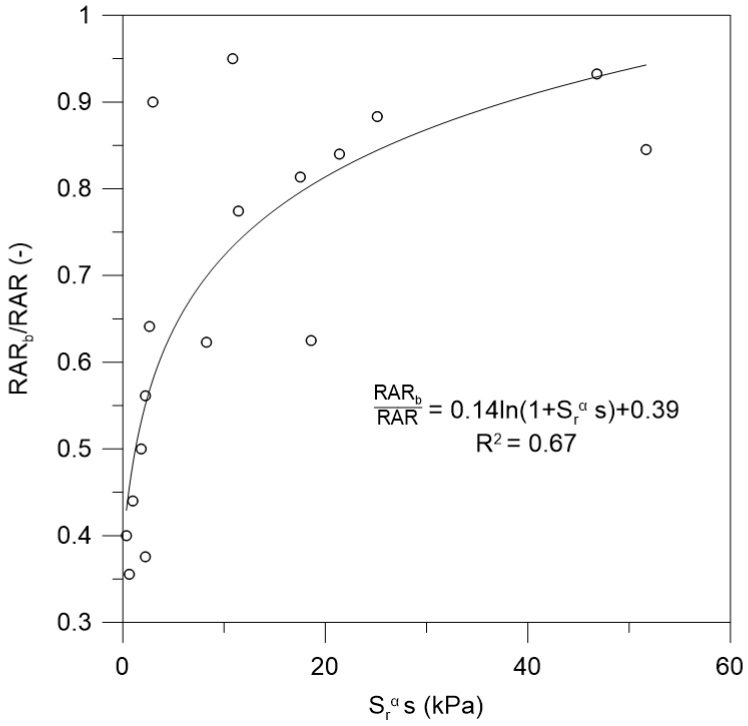

Figure 10 Ratio of broken vs total roots' area as a function of $S_r^{\alpha}s$

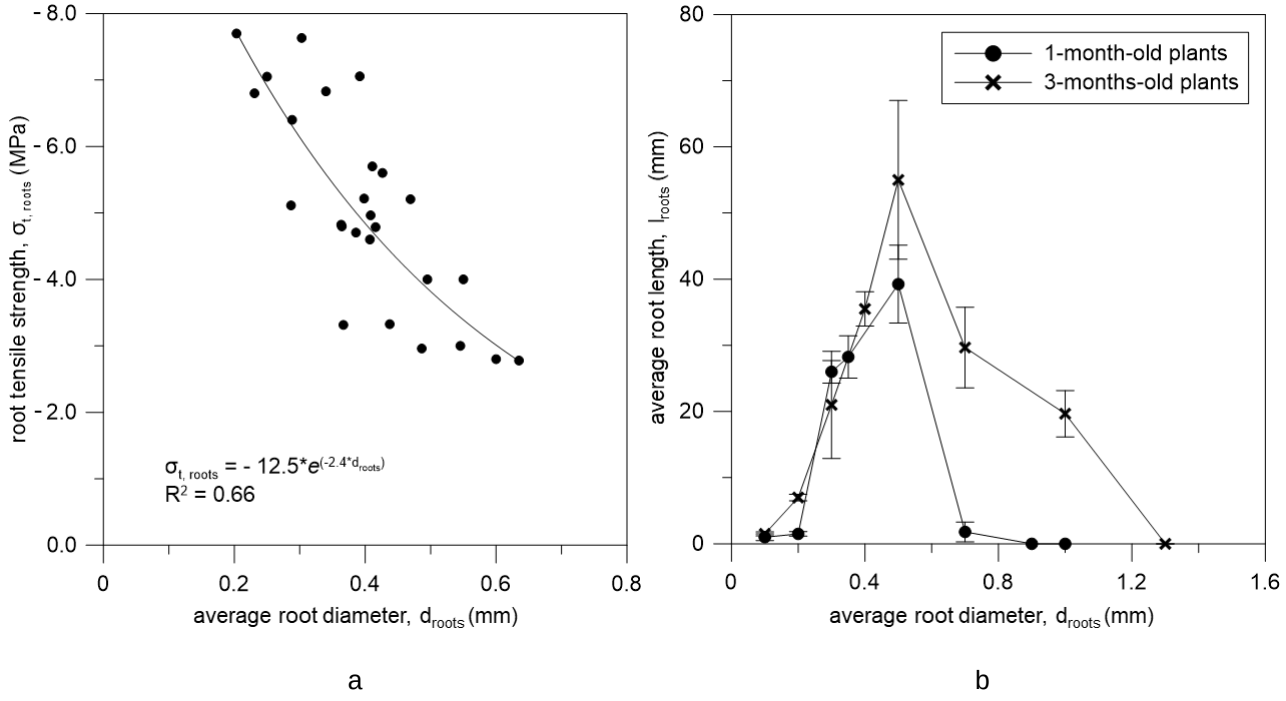

Figure 11 a) Evolution of the root tensile strength as a function of their diameter and b) root average lengths for the different diameter classes (Fraccica, 2019)

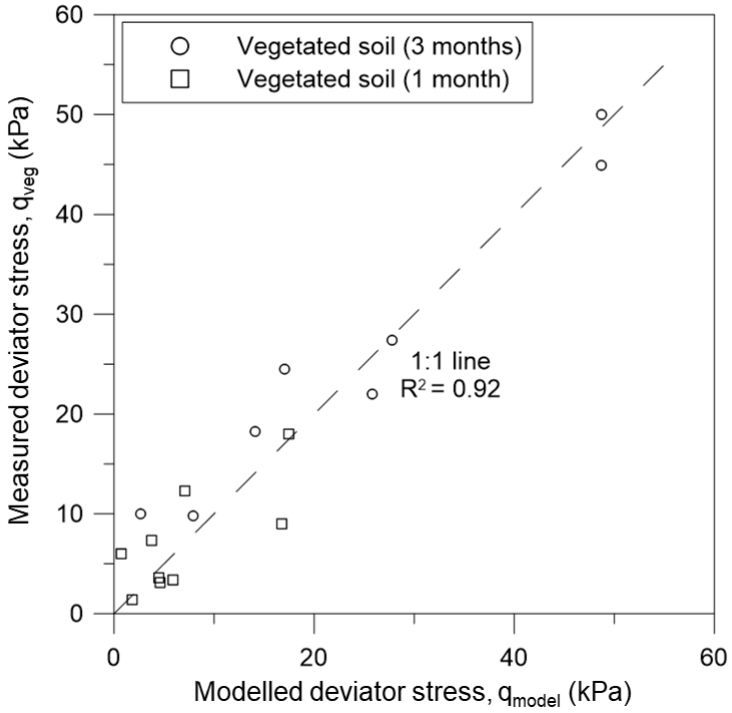

Figure 12 Performance of the model to predict deviator stress in vegetated soil as function of bare soil behaviour and roots morpho-mechanical features.

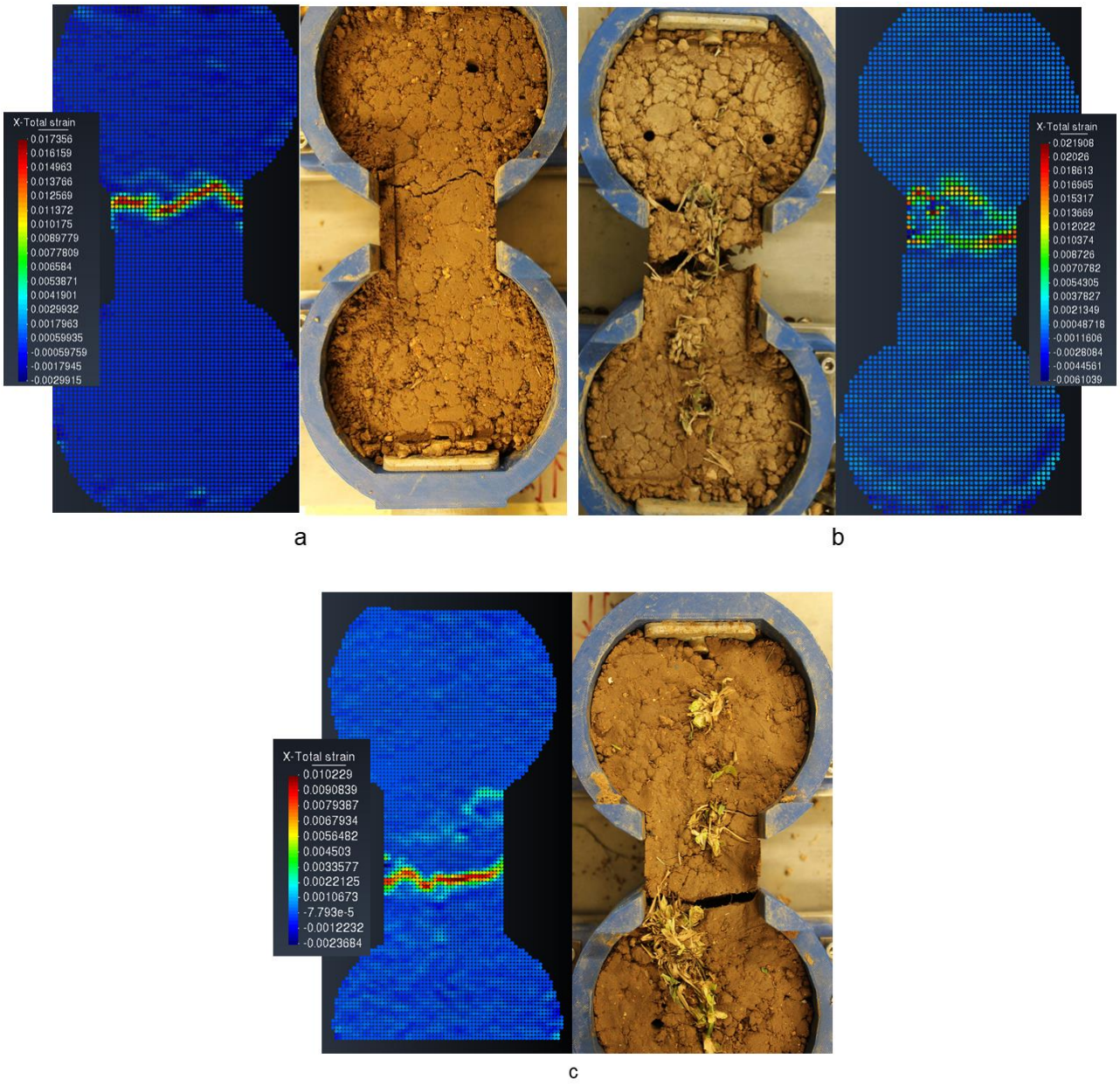

Figure 13 original images and PIV analyses on a) bare soil (s = 15 kPa) and vegetated soil at: b) s = 19.3 kPa and c) s = 100 kPa. Plant shoots removed before testing, to allow better pixels correlation.